Journal of Molecular Structure 1239 (2021) 130463

Contents lists available at ScienceDirect

Journal of Molecular Structure

journal homepage: www.elsevier.com/locate/molstr

Growth dynamics and molecular structural analysis of Dimethylketo thiosemicarbazone single crystals for frequency conversion applications - Optical and thermal characterization

R. Sakunthaladevi [a,c], L. Jothi [b,*]

[a] Department of Physics, Trinity College for Women, Namakkal-637002, Tamil Nadu, India
[b] Department of Physics, N.K.R. Government Arts College for Women, Namakkal-637001, Tamil Nadu, India
[c] Periyar University, Palkalai Nagar, Salem-636011, India

ARTICLE INFO

Article history:
Received 28 February 2021
Revised 2 April 2021
Accepted 7 April 2021
Available online 13 April 2021

Keywords:
Schiff base
X-ray diffraction
Linear and Nonlinear optical studies
Simultaneous thermal studies

ABSTRACT

New organic Schiff base of Dimethylketo thiosemicarbazone (DMKT) was synthesized by condensation process and grown by solvent slow evaporation method in methanol solution. The grown crystal was subjected to a single crystal and powder X-ray diffraction study and to identify that the material crystallized into a triclinic crystal system with a P-1 noncentrosymmetric space group. The X-Ray data reveals that the crystalline network cohesion of this compound. The FT-IR and FT Raman spectral analysis show the vibration behavior of chemical bonds in the grown material. Its optical behavior was examined by UV–VIS spectrum and the DMKT crystal was found to have transparency in the region between 350 nm and 1100 nm. The luminescent emission of the grown material was identified from the fluorescence spectrum. Improvement in the second harmonic generation efficiency of the grown material was studied by the Kurtz and Perry powder method and it shows 26.7 mV of green light emission. The thermal stability and melting point of DMKT were confirmed by various thermal analyses.

1. Introduction

Organic molecular materials have many potential applications in photonics, integrated optics, and the diode laser frequency doubles. Direct frequency doubling of semiconductor diode lasers offers a variety of applications like optical storage, optical chemistry, underwater communication, etc. The important properties of such applications were its transparency, second harmonic generation efficiency, phase matching, etc. [1-2]. One of the advantages in working with organic materials is they have large structural diversity so it was altering their structure, to increase their NLO properties of its pure one [3]. This will increase their desired nonlinear optical properties of the material like second harmonic generation, optical rectification, and parametric amplification [4]. The second harmonic generation is a phenomenon produced by the second-order nonlinearities in a material when it is exposed to high intensity and monochromatic light sources [5]. Organic Schiff bases were synthesized by condensation between a primary amine and an aldehyde or ketone to form an azomethine or imine (-C=N-) group. This is due to the presence of a very high polar carbonyl group [6]. Which have attracted considerable attention due to their wide-ranging applications, like liquid crystals, organic dyes, catalysts, and as intermediates for many bioactive molecules [7]. In nonplanar Schiff base compounds exhibit photochromism and such materials realized in various areas such as radiation control, radiation measurement, optical computers, and display systems [8]. Some of these types of materials have been already reported by many researchers [9-13]. At the same time condensation of aromatic aldehydes or ketones with thiosemicarbazides extend the electron delocalization along with the azomethine and donor sites in the ketonic part which offers much more coordination possibilities for the thiosemicarbazone. This coordinating capability of thiosemicarbazides is attributed to the unlimited delocalization of electron density over the N-H, C-S, N-H systems, which is improved by substitution at the position of N. In this various intermolecular or interionic hydrogen bonding have played an important role in constructing supramolecular structures and involves in the generation of noncentrosymmetric structures [14]. The linkage between ketones and thiosemicarbazides yield a keto thiosemicarbazones prompted us to design new Schiff bases [15]. Thiosemicarbazones have received considerable attention because of their unpredictable bonding modes, promising biological implications and structural diversity [16].

* Corresponding author.
E-mail address: jothilakshmanan@gmail.com (L. Jothi).

https://doi.org/10.1016/j.molstruc.2021.130463
0022-2860/

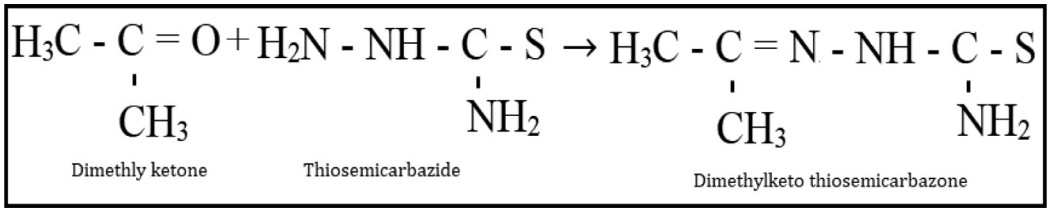

Fig 1. Reaction mechanism of Dimethylketo thiosemicarbazone.

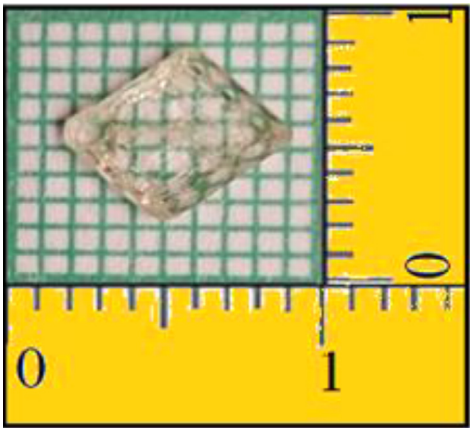

Fig. 2. As grown single crystal of Dimethylketo thiosemicarbazone.

This prompted our study into the synthesis, growth and characterization of dimethylketo thiosemicarbazone (DMKT) single crystals for the first time. The three-dimensional X-ray crystal structure, optical, mechanical and thermal perspectives of these crystals are also presented in this paper. These techniques are very useful for characterizing and identifying various properties of the grown new DMKT material.

2. Experimental procedure

2.1. Material synthesis

The starting compounds are purchased from Sigma Aldrich with 99% purity. Thiosemicarbazide salt was dissolved in methanol solution and start condensing after few minutes, dimethyl ketone was added drop by drop in an appropriate ratio. The chemical reaction was shown in Fig. 1. A supersaturated solution of Dimethylketo thiosemicarbazone was obtained for the continuous condensation of 8 hrs with a temperature of 80 °C.

2.2. Crystal growth

The supersaturated solution was filtered in a beaker by using what mann filter paper. The beaker was kept in an undisturbed position and allowed to solvent slow evaporation at room temperature at atmospheric pressure. Within 20 days a number of seed crystals are visible for a filtered solution in a beaker and after 55 days colourless single crystal of various dimensions is obtained. The grown single crystal of DMKT with the dimension of $7 \times 7 \times 2$ mm^3 was shown in Fig. 2.

2.3. Characterization Techniques

The slightly positive carbon atom in the carbonyl group of ketone can be attacked by a negatively charged ion or a slightly negatively charged part of a molecule in thiosemicarbazide and the carbon-oxygen double bond gets broken and the carbonyl group undergoes addition reactions, with the loss of a water molecule. This reaction is known as addition-elimination or condensation [17]. Based on this the Schiff base of dimethylketo thiosemicarbazone was synthesized.

Table 1
Crystal data and structure refinement parameters for Dimethylketo thiosemicarbazone.

Empirical formula	C4H9N3S
Formula weight	131.20
Temperature	296 (2) K
Wavelength	0.71073 A
Crystal system, space group	Triclinic, P -1
Unit cell dimensions	a = 6.229(4) A, alpha 85.20(4) deg b = 7.8557(2)A, beta = 68.329(2) deg c = 7.987(5)A, gamma = 70.23 deg
Volume	341.4(3) A^3
Z	2
Calculated density	1.271 Mg/m^3
Absorption coefficient	0.376 mm^{-1}
F(000)	140
Crystal size	0.200 × 0.180 × 0.150 mm
Theta range for data collection	3.744 to 36.429 deg
Limiting indices	-10<=h<=10, -13<=k<=13, -13<=l<=13
Reflections collected	21,273
Unique Reflections	3308 [R (int) = 0.064]
Completeness to theta = 25.00	98.5 %
Absorption correction	Semi-empirical from equivalents
Max. and min. transmission	0.7471 and 0.6053
Refinement method	Full – matrix least-squares on F^2
Data / restraints / parameters	3308 / 4/ 86
Goodness-of-fit on F^2	1.086
Final R indices [I>2sigma(I)]	R1 = 0.0523, wR2 = 0.1485
R indices (all data)	R1 = 0.0717, wR2 = 0.1711
Extinction coefficient	0.34(8)
Largest diff. peak and hole	0.402 and -0.389 $e.A^{-3}$

Their physicochemical properties were investigated by using various structural, optical and thermal analyses. The selected crystal was employed in Bruker D8 VENTURE SC-X ray diffractometer and radiated by a source of Mo($K\alpha$) radiation with the help of an attached accurate goniometer. The PHOTON 100 CMOS detector is optimized for the detection of radiations by single crystal X-ray diffraction. Accurate unit cell parameters were refined by the selection of 3308 unique reflections out of 21,273 total reflections. Data collection was performed by using the APEX3 software program and the structure refined by Full-matrix least-squares were given in Table 1.

In powder XRD, a monochromatic X-ray beam was focused on the powder sample having a diameter less than 10 μm to determine structural information in the crystal lattice. It was also used to analyze materials identity, crystallinity, residual stress and textural features with minimum invasion [18]. Interactions of incident X-rays with the sample atomic planes create diffracted, transmitted, refracted, scattered and absorbed beams according to Bragg's law [19] $2d\sin\theta = n\lambda$, which relates the order of diffracted beam (n), the wavelength of the incident X-ray beam (λ) to the distance between nearatomic planes (d-spacings) and the angle of the inci-

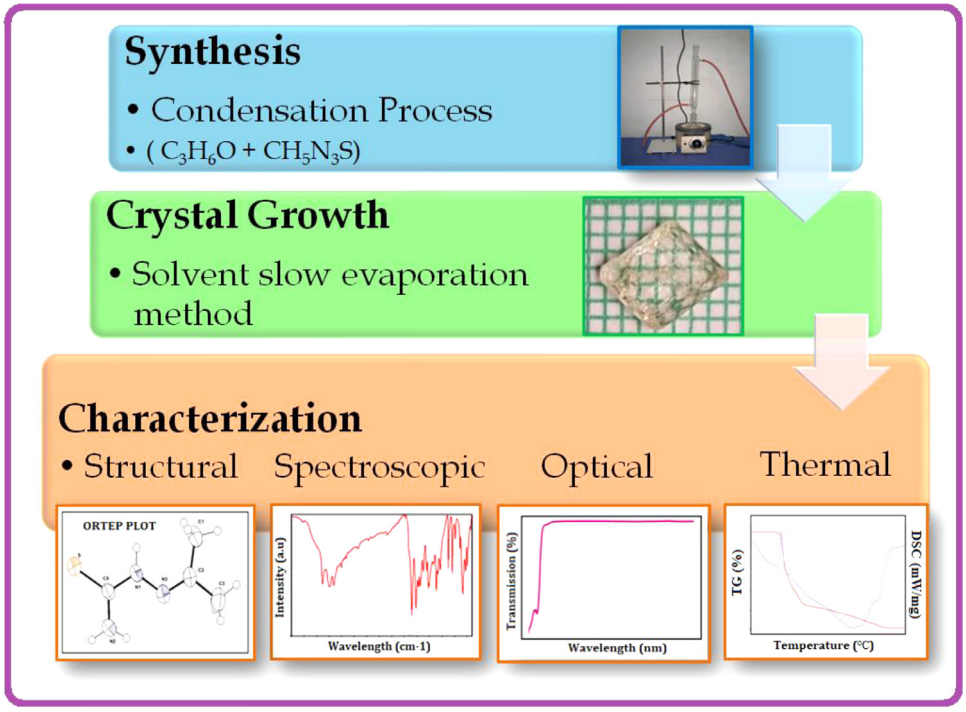

Fig. 3. Schematic diagram of Dimethylketo thiosemicarbazone single crystal.

dence (θ). Changeover of diffracted patterns into d-spacings allows recognition of the unknown sample and was identified by comparing the diffracted pattern beams with many reference patterns stored in the JCPDS library or XRD textbooks [20-24]. Using Rigaku Ultima III X-ray diffractometer and the diffracted beam were detected.

A Perkin Elmer-Paragon Fourier Transform Infrared Spectrometer was used to record the infrared vibrational spectrum of DMKT. The spectrum was recorded by the KBr pellet technique in the ranges from 4000 cm^{-1} to 400 cm^{-1}. Fourier Transform Raman spectrum of DMKT was recorded in the region of 4000–500 cm^{-1} by using Bruker RFS 27 FT-Raman spectrometer equipped with FRA-106 model.

Internal optical transmittance of DMKT material was recorded using Perkin Elmer Lambda 35 UV–VIS spectrometer in the wavelength range of 200–1100 nm. The fluorescence emission spectrum of DMKT was recorded by using Perkin Elmer LS 45 fluorometer. Among the various NLO effect, the frequency doubling or second harmonic generation ability of a material can be analyzed by using the Kurtz Perry powder method. In this method the crystal has been powdered with the uniform particle size and tightly packed in a microcapillary tube of a uniform bore. The tube was mounted in the path of the Q-switched Nd: YAG laser beam emitting a wavelength of 1064 nm, with a power of 1.2 mJ [25]. The output was collected in a monochromator with an IR blocking filter. A photomultiplier was used to detect the out coming green light and the optical signal was converted into voltage output at the cathode ray oscilloscope.

The melting point and mass change due to temperature was analyzed by using various thermal analysis. The differential scanning calorimetry (DSC) measurement for DMKT was carried out by using a sample of 15 g with a NETZSCH DSC 204 F1 PHOENIX thermal analyzer and to get simultaneous TG-DSC and TG-DTG thermal traces by NETZSCH STA 449 F3 Jupiter thermal analyzer. Schematic diagram of Dimethylketo thiosemicarbazone single crystal is shown in Fig. 3

Table 2
Atomic coordinates (x 10^4) and equivalent isotropic displacement parameters ($Å^2$ x 10^3) for Dimethylketo thiosemicarbazone.

	x	y	z	U(eq)
S	1865(1)	4432(1)	2144(1)	49(1)
C(1)	3073(3)	1368(2)	7911(2)	57(1)
C(2)	5396(3)	1640(2)	6699(2)	43(1)
C(3)	7539(4)	962(3)	7297(3)	66(1)
C(5)	4200(2)	3681(2)	2925(2)	38(1)
N(1)	3802(2)	3013(2)	4579(2)	44(1)
N(2)	6456(2)	3659(2)	1962(2)	50(1)
N(3)	5756(2)	2386(2)	5173(2)	45(1)

Table 3
Hydrogen bonds for Dimethylketo thiosemicarbazone [A and deg.].

D-H...A	d(D-H)	d(H...A)	d(D...A)	<(DHA)
C(1)-H(1B)...S#1	0.96	2.79	3.683(3)	155.8
C(3)-H(3C)...S#2	0.96	2.91	3.838(2)	162.7
N(1)-H(1)...S#1	0.916(16)	2.754(19)	3.550(2)	145.9(19)
N(2)-H(2A)...S#3	0.848(14)	3.015(19)	3.674(3)	136.2(17)
N(2)-H(2B)...S#4	0.861(14)	2.582(15)	3.436(2)	171.4(19)

3. Result and Discussion

3.1. X-Ray Diffraction Studies

Suitable crystals of DMKT with dimension 0.2 × 0.18 × 0.15 mm^3 were selected for single crystal X-ray diffraction analysis. From the result, DMKT crystallized into the triclinic system with P1 space group. The atomic coordinates and isotropic displacement parameters of DMKT was given in Table 2. In the unit cell, the packing of molecules was stabilized by the interaction of hydrogen bonding between them and the observed interactions are given in Table 3 and the interactions were C_1-H_{1B}...S_1, C_3-H_{C3}...S_2, N_1-H_1...S_1, N_2-H_{A2}...S_3, and N_2-H_{B2}...S_4. The

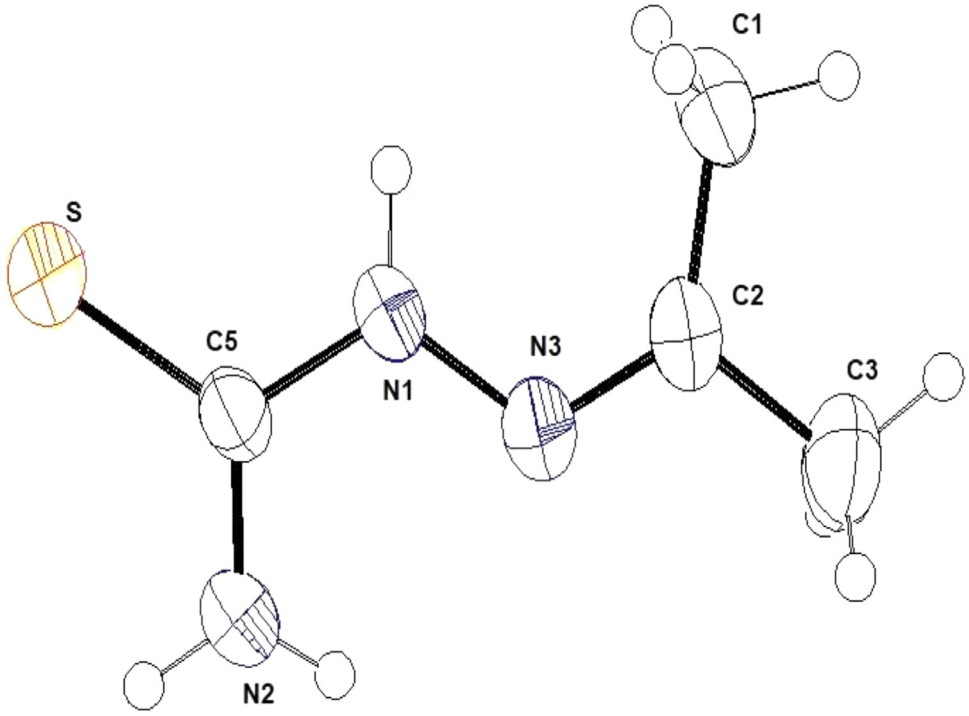

Fig. 4. ORTEP plot of Dimethylketo thiosemicarbazone with 50% probability.

Table 4
Bond lengths [A] and Bond angles [deg] for Dimethylketo thiosemicarbazone.

S-C(5)	1.6975(16)	C(2)-C(1)-H(1A)	109.5
C(1)-C(2)	1.489(2)	C(2)-C(1)-H(1B)	109.5
C(1)-H(1A)	0.9600	H(1A)-C(1)-H(1B)	109.5
C(1)-H(1B)	0.9600	C(2)-C(1)-H(1C)	109.5
C(1)-H(1C)	0.9600	H(1A)-C(1)-H(1C)	109.5
C(2)-N(3)	1.2833(19)	H(1B)-C(1)-H(1C)	109.5
C(2)-C(3)	1.498(2)	N(3)-C(2)-C(1)	126.35(14)
C(3)-H(3A)	0.9600	N(3)-C(2)-C(3)	116.40(15)
C(3)-H(3B)	0.9600	C(1)-C(2)-C(3)	117.24(14)
C(3)-H(3C)	0.9600	C(2)-C(3)-H(3A)	109.5
C(5)-N(2)	1.3247(19)	C(2)-C(3)-H(3B)	109.5
C(5)-N(1)	1.3462(18)	H(3A)-C(3)-H(3B)	109.5
N(1)-N(3)	1.3897(18)	C(2)-C(3)-H(3C)	109.5
N(1)-H(1)	0.916(16)	H(3A)-C(3)-H(3C)	109.5
N(2)-H(2A)	0.848(14)	H(3B)-C(3)-H(3C)	109.5
N(2)-H(2B)	0.861(14)	N(2)-C(5)-N(1)	117.22(13)
		N(2)-C(5)-S	123.26(11)
		N(1)-C(5)-S	119.47(11)
		C(5)-N(1)-N(3)	118.17(12)
		C(5)-N(1)-H(1)	119.3(15)
		N(3)-N(1)-H(1)	121.2(15)
		C(5)-N(2)-H(2A)	119.9(14)
		C(5)-N(2)-H(2B)	119.4(14)
		H(2A)-N(2)-H(2B)	120.1(17)
		C(2)-N(3)-N(1)	117.54(13)

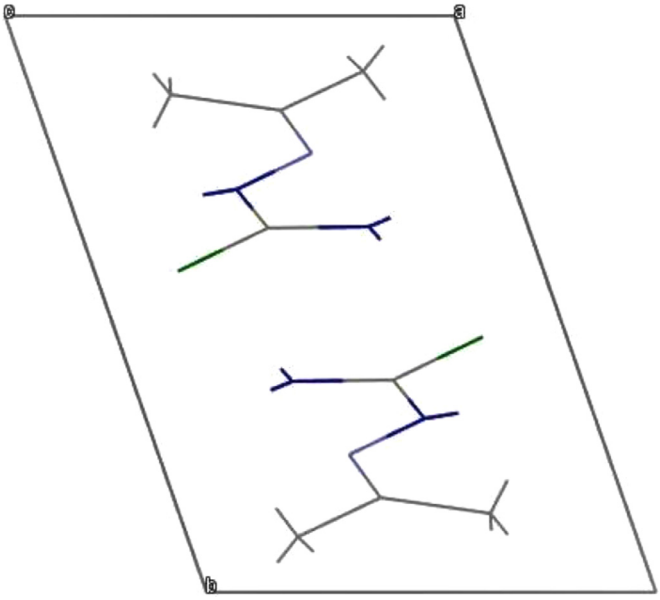

Fig. 5. Unit cell diagram of Dimethylketo thiosemicarbazone.

selected bond lengths and bond angles were given in Table 4. Some thiosemicarbazone derivatives, the N-N bond lengths were reported in the range 1.3782–1.389 Å [26], 1.3866 Å [27], 1.3894 Å [28], 1.3966 Å [29].

For the title compound, the N-N bond length was 1.3897 which is due to an N-N single bond and N=N double bond. The bond at 1.2833 shows the typical double bond between C_2=N_3 and a single bond of C_5-N_2, C_5-N_1 was obtained at 1.3247 Å and 1.3462 Å respectively. This is smaller than the normal C-N single bond length of about 1.48 Å this is due to the effect of resonance in the molecule [30]. The ORTEP plot of the molecules in the title compound with displacement ellipsoids were drawn 50% probability and shown in Fig. 4.

The Unit cell and hydrogen bonding diagram of the grown DMKT crystal along the b-axis were given in Fig. 5 and 6 respectively. The bond length between S-C_5 is 1.6975 Å and the bond angles are C_5-N_1-N_3 = 118.17°, N_2-C_5-S = 123.26°, N_1-C_5-S = 119.47° and N_2-C_5-N_1 = 117.22°.

Anisotropic displacement parameters of the form $-2\pi^2$ [$h^2a^{*2}U_{11}$+...+2hka*b*U_{12}] were given in Table 5. Different hydrogen coordinates with their corresponding isotropic displacement parameters were given in Table 6. The various tensional angles C_5-N_1-N_3-C_2 = -175.39°, N(2)-C(5)-N(1)-N(3) = 1.3(2),

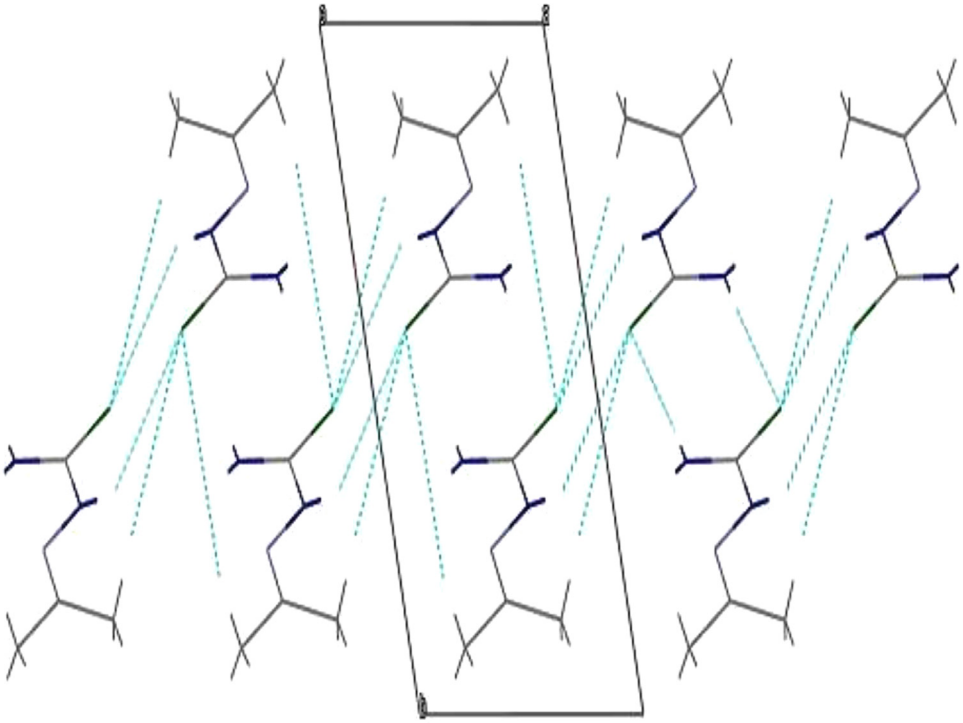

Fig. 6. Hydrogen bonding diagram of Dimethylketo thiosemicarbazone.

Table 5
Anisotropic displacement parameters (A^2 x 10^3) for Dimethylketo thiosemicarbazone.

Atom	U11	U22	U33	U23	U13	U12
S	48(1)	63(1)	37(1)	16(1)	-17(1)	-19(1)
C(1)	65(1)	60(1)	44(1)	18(1)	-20(1)	-22(1)
C(2)	56(1)	39(1)	38(1)	6(1)	-23(1)	-15(1)
C(3)	76(1)	72(1)	66(1)	19(1)	-46(1)	-26(1)
C(5)	43(1)	37(1)	30(1)	6(1)	-11(1)	-12(1)
N(1)	43(1)	52(1)	32(1)	12(1)	-12(1)	-14(1)
N(2)	45(1)	62(1)	38(1)	16(1)	-13(1)	-19(1)
N(3)	49(1)	49(1)	40(1)	10(1)	-19(1)	-17(1)

Table 6
Hydrogen coordinates ($\times$ 10^4) and isotropic displacement parameters $Å^2x10^3$).

Atom	x	y	z	U(eq)
H(1A)	3297	778	8966	85
H(1B)	1796	2520	8262	85
H(1C)	2628	628	7288	85
H(3A)	7071	434	8448	98
H(3B)	8857	65	6429	98
H(3C)	8064	1953	7400	98
H(1)	2230(30)	3200(30)	5360(30)	70(7)
H(2A)	7540(30)	3350(30)	2440(30)	56(6)
H(2B)	6760(40)	4100(30)	910(20)	57(6)

S-C(5)-N(1)-N(3) = 179.14(10), C(1)-C(2)-N(3)-N(1) = 0.3(2), C(3)-C(2)-N(3)-N(1) = 179.46(14) and C(5)-N(1)-N(3)-C(2) = -175.39(13) were listed in Table 7. There is a difference in torsion angles of the same bonding C-C-N-N= 0.3 and 179.46 indicates the presence of asymmetric units in the DMKT crystal.

3.2. Powder XRD Studies

The powder sample of the grown crystal was scanned over various 2θ values from 0° to 60° at a rate of 1° per min. The d spacing for each diffraction peak in the spectrum was identified from the powder X ray diffraction pattern. The sharp and well-defined Bragg's peaks confirmed the high crystallinity of the grown crystals and some low-intensity peaks also present. Powder X-ray diffraction pattern of the grown DMKT crystals was shown in Fig. 7.

Pure thiosemicarbazone shows sharp single diffraction peak at 17.25° and 28.21° [30] but in DMKT spectrum shows a prominent peaks at 13.01°, 16.85° and 27.58°. The powder X-ray diffraction pattern of DMKT showed triplet in between 24° to 25° but in the pure compound only one peak was obtained at 24.6°. These little bit shift of peaks was due to the addition of dimethyl ketone to thiosemicarbazone.

Table 7
Torsion angles [degree] found in Dimethylketo thiosemicarbazone.

N(2)-C(5)-N(1)-N(3)	1.3(2)
S-C(5)-N(1)-N(3)	179.14(10)
C(1)-C(2)-N(3)-N(1)	0.3(2)
C(3)-C(2)-N(3)-N(1)	179.46(14)
C(5)-N(1)-N(3)-C(2)	-175.39(13)

3.3. Fourier Transform Infrared Vibrational studies

From FTIR spectrum is shown in Fig 8 the peaks in the region 2950–3050 cm^{-1}, 2935–2995 cm^{-1}, 1400–1510 cm^{-1} and 1275–1425 cm^{-1} were vibrations of the CH_2 group in asymmetric stretching, symmetric stretching, scissoring and wagging respectively [31,32]. The overlapping spectra of a methyl group (CH_3) obtained in the region of 3000–2940 cm^{-1} and 2960–2310 cm^{-1} were two C-H bonds in the methyl group are contracting and one C-H bond was contracting [31]. The grown compound shows these peaks at 2998 cm^{-1} and 2458 cm^{-1}. The asymmetric and symmetric stretching vibrations of NH_2 give rise to a band in the region of 3420–3330 cm^{-1} and in between 3150–3270 cm^{-1} in the present work, it was observed at 3377 cm^{-1} and 3152 cm^{-1} [33]. The band in the region of 3450–3330 cm^{-1} appears due to NH stretching

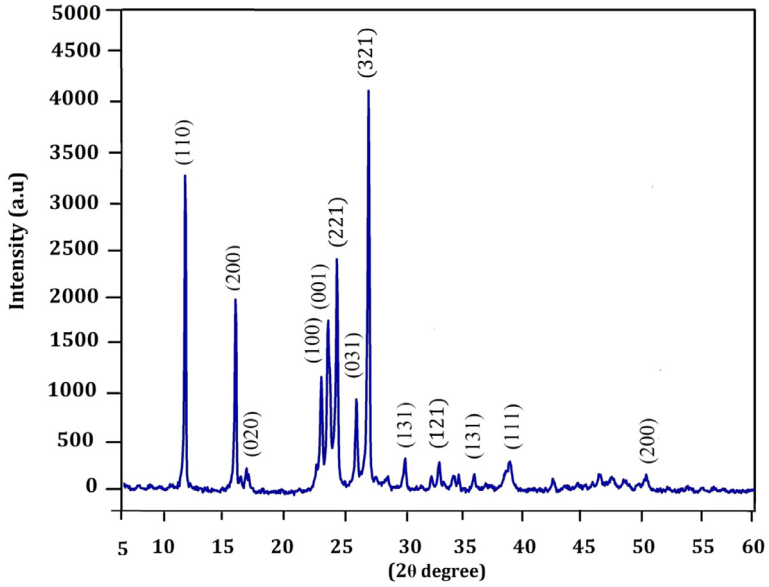

Fig. 7. Powder X-ray diffraction pattern of Dimethylketo thiosemicarbazone.

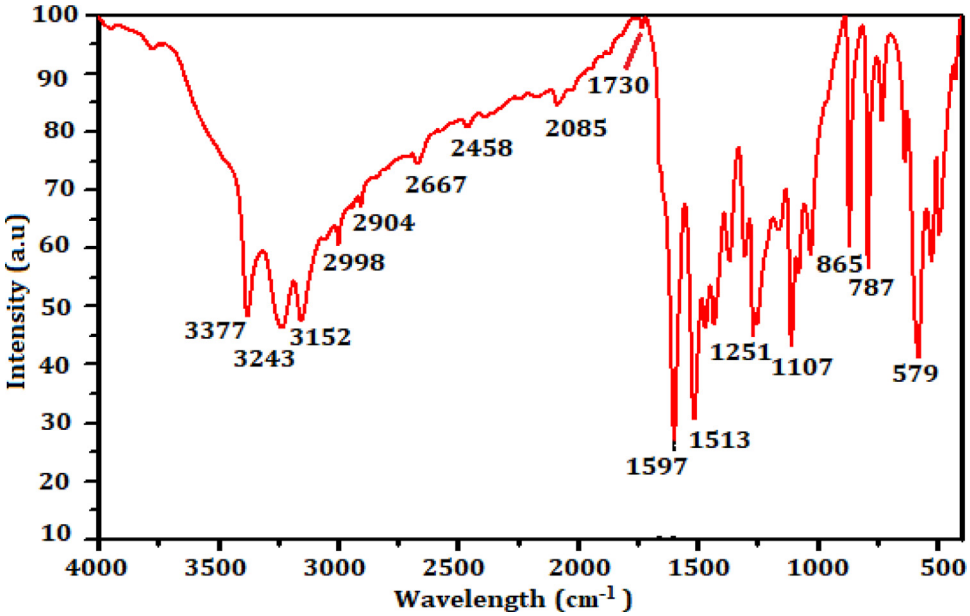

Fig. 8. Fourier Transform Infrared spectrum of Dimethylketo thiosemicarbazone.

vibration wherein the DMKT compound it appears at 3377 cm^{-1} [34].

The C=N stretching skeletal bands observed in 1650–1550 cm^{-1} [35, 36] which was 1597 cm^{-1} in the spectrum of DMKT and confirms the formation of Schiff base. The C-N stretching vibration coupled with NH in-plane bending active in the region of 1320–1225 cm^{-1} [37] and was observed at 1268 cm^{-1} and 1251 cm^{-1}. The out-of-plane bending of N-N was observed at 1076 cm^{-1} in the range of 1037–1083 cm^{-1} [38]. The C=S stretching vibrations were observed in the range of 670–930 cm^{-1} [39], and which was obtained at 865 cm^{-1} for the title compound.

3.4. Fourier Transform Raman Vibrational studies

The FT Raman spectrum of a powdered sample of DMKT was recorded. The overlapping spectra of methyl group CH_3 obtained in 3002 cm^{-1}, 2938 cm^{-1} due to asymmetric stretching and 2905 cm^{-1}, 2722 cm^{-1} due to symmetric stretching. From Fig. 9 the sharp peak at 1644 cm^{-1} was assigned as C=N stretching mode [40]. The in-plane bending of NH_2 was observed at 1593 cm^{-1} and the band in 1076 cm^{-1} was due to NH_2 rocking. The N and H atom in CNH moves in the same direction as carbon atom in the amide group appear at 1434 cm^{-1} and in opposite direction appear at 1292 cm^{-1} [41]. The stretching of C=S mode was observed at 863 cm^{-1} [42] and out-of-plane the rocking of NH was observed at 712 cm^{-1} [43]. Table 8 gives the observed FT-IR and FT Raman bands with wavenumbers and the corresponding assignments.

3.5. Optical Transmission spectral analysis

An optically polished crystal of 1 mm thickness was used for recording the optical transmission spectrum of DMKT and shown in Fig. 10. The optical absorption coefficient (α) was used to find,

Extinction coefficient $K = \frac{\propto}{4\pi}$,

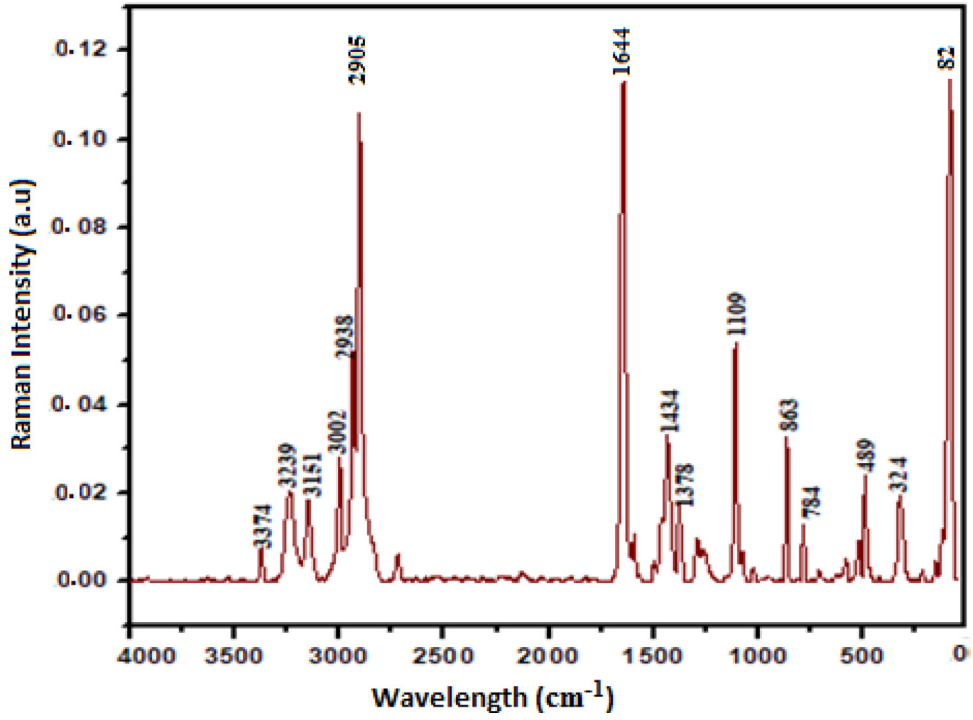

Fig. 9. Fourier Transform Raman spectrum of Dimethylketo thiosemicarbazone.

Table 8
Wave numbers and assignments of FT-IR and FT Raman bands of Dimethylketo thiosemicarbazone.

FTIR (cm^{-1})	FT-Raman (cm^{-1})	Spectral Assignments
3377	3374	NH stretching
2998	3002	CH_3 stretching
-	2938	CH_3 asymmetric stretching
2904	2905	CH_3 symmetric stretching
1597	1644	C=N stretching
1513	1498	NH in plane bending
1466	1463	CH_3 asymmetric stretching
1429	1434	CH_3 in plane bending
1366	1378	CH_3 in plane bending
1301	1292	CN stretching
1107	1109	NN rocking
1076	1082	NH_2 rocking
1026	1035	NH rocking
865	863	CS stretching
634	612	NH wagging
579	-	CC in plane bending
-	582	CN in plane bending
492	489	CNH out of plane bending
-	324	CS out of plane bending
-	223	NH_2, CH_3 torsion
-	82	CNN out of plane bending

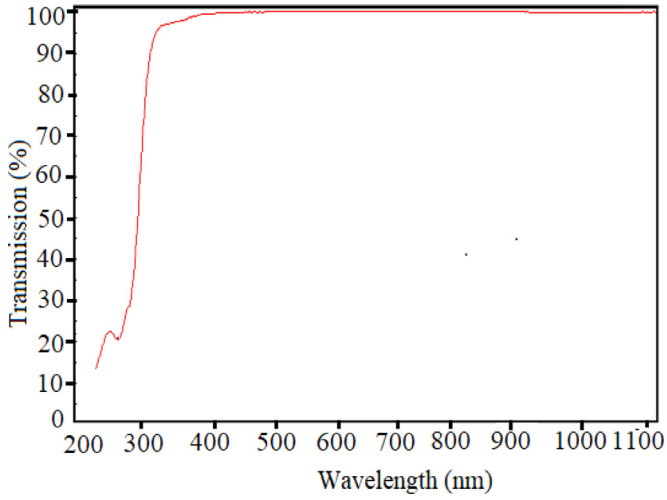

Fig. 10. UV – VIS Transmission spectrum of Dimethylketo thiosemicarbazone.

$$\text{Bandgap energy } E_g = \frac{1240}{\lambda}(\text{eV}) \text{ and}$$

$$\text{Urbach energy } E_u = \frac{h\nu}{\log \alpha}(eV),$$

where λ is the lower cut-off wavelength of the sample and where h is Plank's constant [44-46]. Bandgap energy was the difference in energy between the valence band and the conduction band of a solid material it is simply the energy of forbidden electrons movement in the material. Urbach energy was governed by the structural disorder, an imperfection in stoichiometric and passivation at the surface and the disorder of phonon states. It is inversely proportional to the bandgap energy [47]. From the UV–VIS spectrum, it shows variations in transmission below 350 nm and above 350 nm it shows 99%, which proves the optical linearity of the DMKT crystal. The lower cut of wavelength was observed at 223 nm this is due to interband electronic transitions [48]. Using the lower cut-off wavelength bandgap energy value was calculated as 5.6 eV which is shown in Fig. 10. Also using a Tauc's plot E_g was obtained as 5.55 eV and shown in Fig. 11. The variation of extinction coefficient K with photon energy was shown in Fig. 12 and a sharp rising between 5 to 6 eV indicates the bandgap energy present in this region. The high transmission of the grown crystal in the entire visible region with a wide bandgap indicates the low defect concentration in the grown material [49]. Urbach energy was calculated from Fig. 13 and the value was 2.02 eV. The bandgap energy and Urbach energy were important parameters for designing devices in optical communication technology [50].

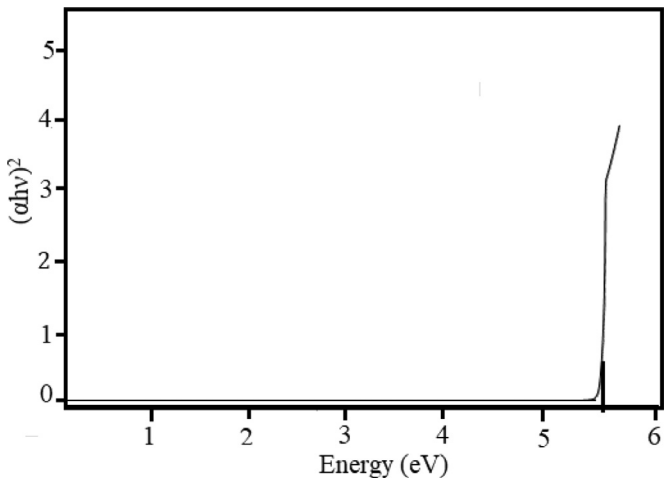

Fig. 11. Tauc's plot of Dimethylketo thiosemicarbazone.

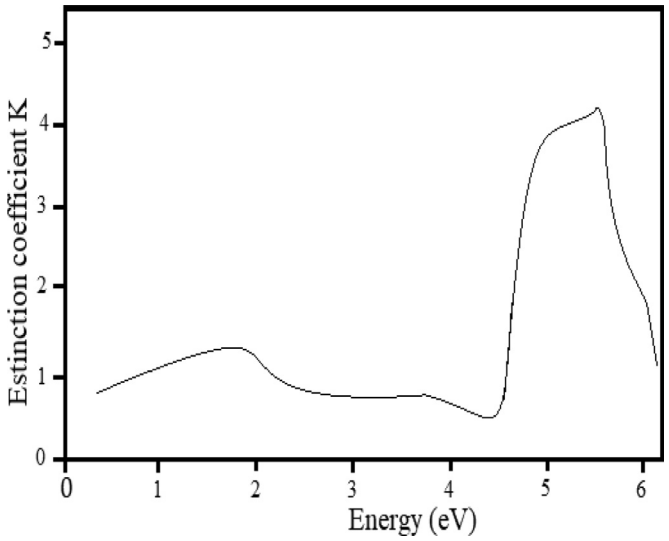

Fig. 12. Plot of extinction coefficient K vs phton energy hν for Dimethylketo thiosemicarbazone.

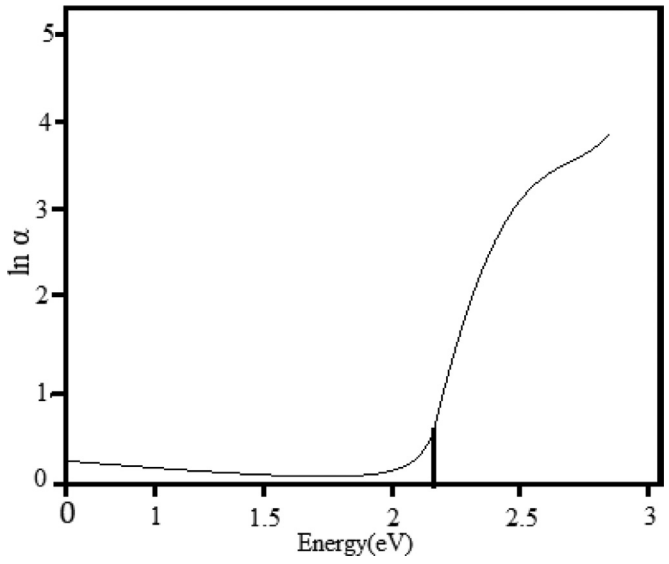

Fig. 13. Plot of lnα vs phton energy hν for Dimethylketo thiosemicarbazone.

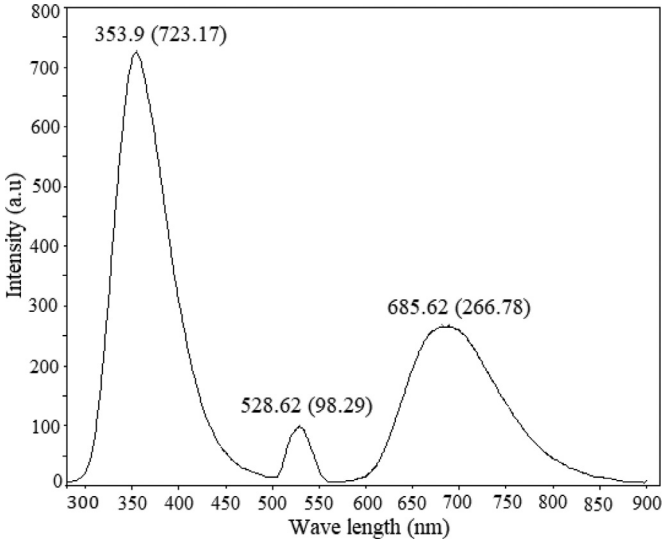

Fig. 14. Fluorescence emission spectrum of Dimethylketo thiosemicarbazone.

3.6. Fluorescence spectral analysis

Fluorescence spectral analysis provides information about the luminescent behaviors of the grown optical materials in a solid state at room temperature. Excitation transitions of electrons from the ground to the various excited states result in the occurrence of various peaks in the fluorescence emission spectrum [51]. Fig. 14 shows the fluorescence spectrum of DMKT and three emission peaks with different intensities in the wavelength range of 280–900 nm were obtained. The first sharp peak appears at a wavelength of 353 nm with high intensity, the second small peak appears at 528 nm with low intensity and the third medium peak at 685 nm with medium intensity. From these, the grown DMKT shows three types of emissions, emits ultraviolet color with an intensity of 723 a.u and the wavelength range from 300 to 450 nm. The green color with an intensity of 98 a.u was observed in the range between 500 and 550 nm. Finally, red color with an intensity of 266 a.u was emitted in the wavelength range from 600 to 850 nm. The properties of emission correlated with the intermolecular interactions which yield molecular conformation, the supramolecular structure of fluorescent crystals and controllable crystal engineering [52].

3.7. Second harmonic generation efficiency studies

The nonlinear optical properties of a material are due to the nonlinear polarization of light in the homogeneous but moderate electric field. In this way, the number of bonds especially hydrogen bonding in material in solid-state may impact the NLO properties significantly [53]. Several NLO phenomena can occur when intense light interacts with non-absorbing media, resultant in the formation of new beams of dissimilar wavelengths [54]. In addition to identifying the materials with noncentrosymmetric crystal structure, and used to identify the materials phase matching capacity [55]. The only noncentrosymmetric crystal structure can exhibit the SHG and it was confirmed by the emission of green light. The output of green light with voltage 26.7 mV and 22 mV were obtained by DMKT and KDP crystals respectively. This notable frequency doubling of the grown DMKT was attained due to the formation of electronic sub energy band below the bandgap and promoting more electron-proton interaction and hence it can be used in laser industry [56, 57].

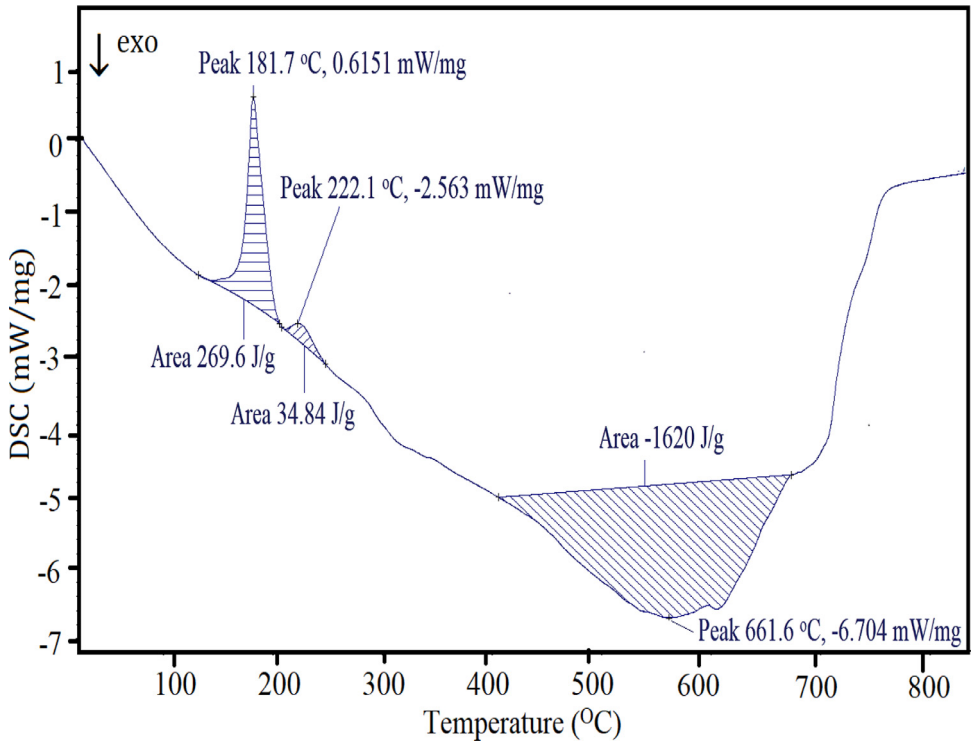

Fig. 15. Differential Scanning Calorimetric trace of Dimethylketo thiosemicarbazone.

3.8. Thermal analysis

Considerate the essential thermal properties of a given material was an important part of material design and study. Thermal analytical methods analysis changes in the physical and chemical effects of material as a function of temperature [58]. It can provide the typical transformation temperatures of the process (quality characteristics) and derivative values proportional to the quantity of the transformed material can be obtained [59]. A tool to explore material thermal properties was large, one of these was differential scanning calorimetry (DSC) which measures the heat flow of a sample during heating (or cooling). It is useful for the determination of several thermodynamic properties of a material such as the melting and freezing temperatures, the specific heat, the phase change, enthalpies, etc. [60]. The initial temperature at which a transformation takes place as shown by the intersection of the extension of the baseline and the tangent to the inflection point.

Fig. 15 gives the DSC trace of the grown DMKT material, which is obtained by the temperature versus difference in heat flow. The heat flow differential was found between the test sample and the reference cell due to the absorbed or released heat as a function of constant heating rate and was registered as a temperature differential ratio.

The formula for the DSC heat flow was measured as [61],

$$\frac{dH}{dt} = \mathrm{Cp}\frac{dT}{dt} + \mathrm{f(T,\,t)}$$

where C_P is sample heat capacity, $\frac{dT}{dt}$ is the heating rate and f (T, t) is heat flow at a function of time at an absolute temperature. The first heat flow obtained at 0.6151 mW/mg with an area of 269 J/g at temperature 181 °C, the second flow at 2.563 mW/mg with an area of 34 J/g at temperature 222 °C and the third one were -6.704 with area 1820 J/g at temperature 561 °C. It shows an increase of the DSC intensity in the range near 181 °C. This variation to be related to an increase in molecular weight and stability, so which indicates that the melting point of the grown material [62]. Now a day simultaneous thermal analytical methods were used to record two different parameters to temperature at the same time. The development of TG, coupled with the derivative thermogravimetry (DTG) and differential scanning calorimetry (DSC) was carried out for the DMKT crystals.

The commercial thermal analyzer of simultaneous TG-DTG was widely used for the mechanism of oxidation as fast also easy to operate and relatively cheap [63]. From the simultaneous TG-DTG curve the material decomposes immediately after the melting point of 181 °C due to the gaseous products like N_2, H_2, H_2S, etc. [64]. After that, the increases in mass losses occur in three steps and shown in Fig. 16. A major weight loss of 60.01% in the first step was obtained in the temperature range from 180 °C - 260 °C, which is due to the evaporation of the solvent and the presence of any other volatile matter. In the second step, the weight loss of 23.482 % was obtained in the temperature range from 260 °C - 500 °C, which may be due to the decomposition of the main groups such as NH, CS, CC, etc. In the last stage, the weight loss of 15.17 % was obtained in the temperature range from 500 °C - 750 °C, which may be due to the complete decomposition of the cross-linkage between the two monomer units [64]. At the temperature above 750 °C the sample fully decomposes and a residual mass of 1.32 % was obtained at 832 °C. The residue remains after all the decomposition was due to the presence of carbon residue [65].

The simultaneous TG-DSC results can be difficult to interpret due to the high complexity of the organic matter because a fusion, decomposition and polymerizations can occur together with an increasing temperature, resulting in the superposition of endothermic and exothermic effects [66].

Fig. 17 shows the simultaneous TG-DSC plot of DMKT, from the TG trace the material starts to decompose at 181 °C and a sudden fall of weight occurs in between 181 °C and 300 °C. After 300 °C a gradual decrease in weight was obtained up to 710 °C and finally reached a constant weight loss. Simultaneously in the DSC trace, an endothermic peak was obtained at 181 °C after a sudden fall was

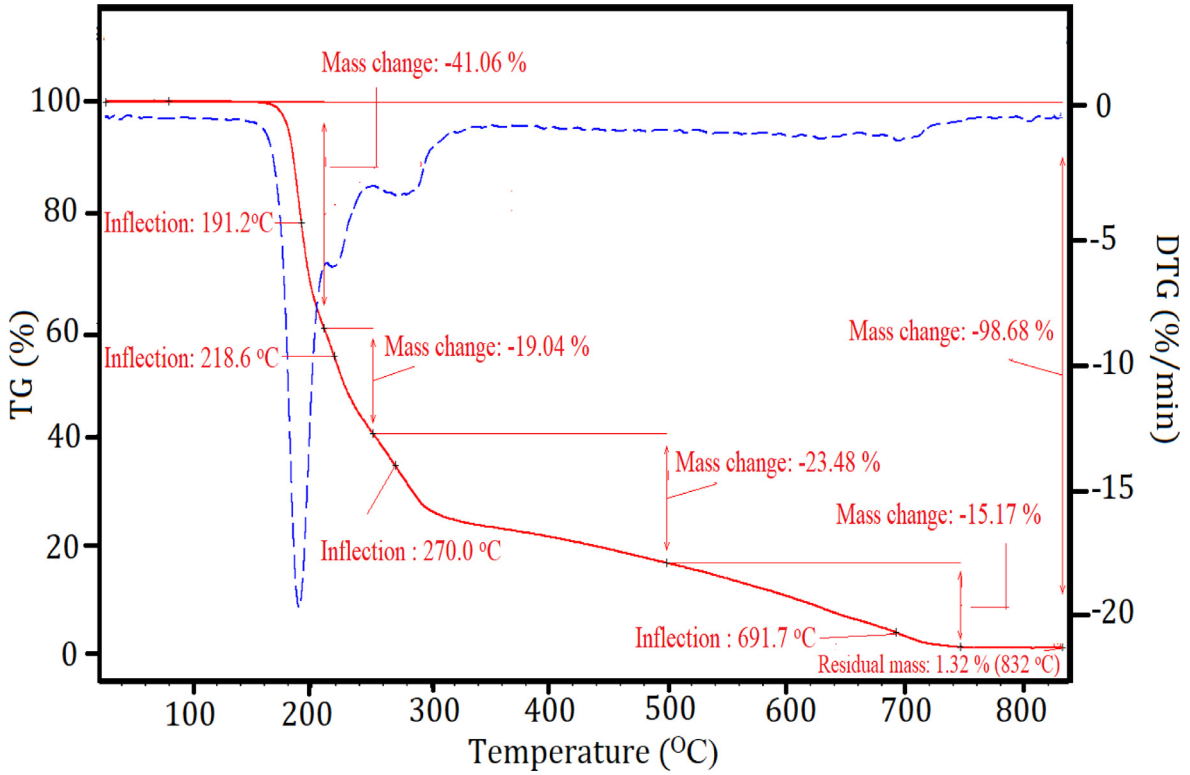

Fig. 16. Simultaneous TG-DTG trace of Dimethylketo thiosemicarbazone.

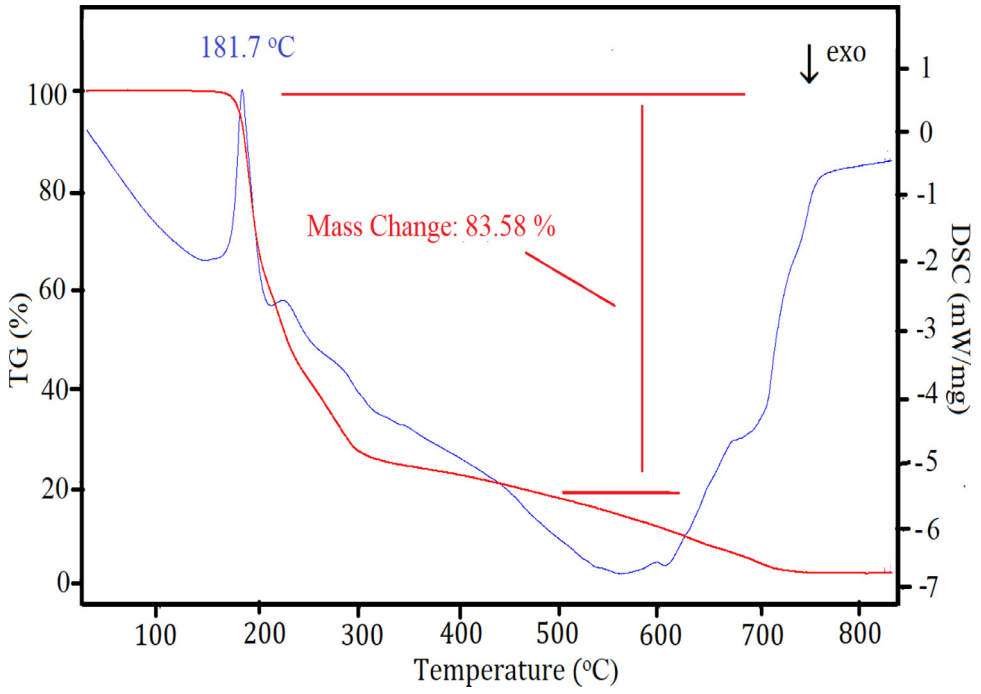

Fig. 17. Simultaneous TG-DSC trace of Dimethylketo thiosemicarbazone.

obtained up to 570 °C and after 600 °C again increases the peak. From all the above studies the melting point of the grown DMKT material was observed at 181 °C and it was lower than the one of the parent compound thiosemicarbazone (183 °C) and higher than the other parent compound dimethyl ketone (-94.7 °C). This confirms the formation and crystallization of the grown DMKT material and up to 181 °C the material was used in NLO applications.

4. Conclusion

An organic Schiff base of Dimethylketo thiosemicarbazone (DMKT) was synthesized by condensation process and an optically good quality single crystal of dimension 7 × 7 × 2 mm^3 was obtained by a solvent slow evaporation method. The single crystal and powder X-ray diffraction (XRD) studies of the grown DMKT confirmed the material be owned to triclinic crystal system with

P-1 space group. The molecular structure and stoichiometry of the DMKT were also elucidated from single crystal XRD studies. The torsion angles of the same bonding C(1)-C(2)-N(3)-N(1) and C(3)-C(2)-N(3)-N(1) with different values reveals the presence of asymmetric units in the grown material. The presence of C=N bonding shows the vibrational frequency band between 1550 cm^{-1} - 1650 cm^{-1} and which was attained by both FT-IR and FT Raman spectra. The linear optical property was studied by using UV–VIS transmission spectrum and it shows 99% transmission in the visible region. The energy gap values calculated from the lower cut-off wavelength was 5.6 eV and from Tauc's plot was 5.55 eV and the value of Urbach energy was 2.02 eV. The fluorescence spectrum shows the luminescent emission functioning of the grown material. The Kurtz-Perry powder method indicates that the SHG efficiency of the DMKT was 1.21 times more than that of KDP. The sharp endothermic peak in DSC trace, a sudden weight loss in simultaneous TG-DTG trace and simultaneous TG-DSC trace all were confirmed the grown DMKT crystal stable up to 181 °C and the compound formed without any water molecule. The spectroscopic, linear, nonlinear optical studies and thermal analysis showed that the grown crystal is a potential candidate for solar cell fabrication, fiber optic communications, laser applications and high temperature measurements.

Declaration of Competing Interest

The authors declare that they have no known competing financial interests or personal relationships that could have appeared to influence the work reported in this paper.

Acknowledgements

The authors thank Sophisticated Instrumentation center, Indian Institute of Technology, Chennai for the support in single crystal XRD, Thermal and FT Raman data collection, Prof. P.K. Das, Indian Institute of Science, Bangalore for having protracted laser facilities for SHG measurements and Archbishop Casimir Instrumentation center, St. Joseph's College, Tiruchirappalli for UV, FT-IR and Fluorescence characterization of the sample.

References

[1] Paolo Bettotti, Hybrid Materials for Integrated Photonics, Adv. Opt. (2014) 1–24.
[2] E.D. D'silva, G. Krishna Podagatlapalli, S. Venugopal Rao, S.M. Dharmaprakash, Structural, optical and electrical characteristics of a new NLO crystal, Opt. Laser Technol. 44 (2012) 1689–1697.
[3] Xiu Liu, Zhou Yang, Dong Wang, Hui Cao, Molecular Structures and Second-Order Nonlinear Optical Properties of Ionic Organic Crystal Materials, Crystals 6 (2016) 158–177.
[4] Christopher H. Hendon, Adam J. Rieth, Maciej D. Korzyński, Mircea Dinca, Grand Challenges and Future Opportunities for Metal–Organic Frameworks, ACS Cent. Sci. 3 (2017) 554–563.
[5] Christoper M. Ashcroft, Jacqueline M. Cole, Handbook of Organic Materials for Electronic and Photonic Devices, second edition, 2019.
[6] L. Jothi, R. Ramesh Babu, K. Ramamurthi, Synthesis, Growth and Characterization of Organic Nonlinear Optical Single Crystals of 4-Bromo-4′-Methyl Benzylidene Aniline, J. Miner. Mater. Char. Eng. 2 (2014) 308–318.
[7] Mohammad Sayed Alam, Dong-Ung Lee, Syntheses, crystal structure, Hirshfeld surfaces, fluorescence properties, and DFT analysis of benzoic acid hydrazone Schiff bases, Spectrochim. Acta A 145 (2015) 563–574.
[8] Ali Mohammed Yimer, Review on Preparation and Description of some First Series Divalent Transition Metal Complexes with Novel Schiff's Base Ligands, Catal. Rev. 2 (2015) 14–25.
[9] K. Senthilkannan, S. Gunasekaran, Spectroscopic Studies and other Novel Studies of 4-Bromo 4′-Chloro Benzylidene Aniline (BCBA) Crystal: A Non Linear Optical Material, Int. J. Chemtech Res. 5 (2013) 3051–3058.
[10] K. Srinivasan, R. Biravaganesh, R. Gandhimathi, P. Ramasamy, Growth and characterization of NMBA (4-nitro-4′-methyl benzylidene aniline) single crystals, J. Cryst. Growth 236 (2002) 381–392.
[11] L. Jothi, G. Vasuki, R. Ramesh Babu, K. Ramamurthi, Synthesis, crystal growth and characterization of organic NLO material: 4-Bromo-4-hydroxybenzylidene aniline, Optik 125 (2014) 2017–2021.
[12] A. Subashini, R. Kumaravel, S. Leela, Helen Stoeckli Evans, D. Sastikumar, K. Ramamurthi, Synthesis, growth and characterization of 4-bromo-4-chloro benzylidene aniline: A third order non linear optical material, Spectrochim. Acta A 78 (2011) 935–941.
[13] R Sakunthaladevi, L Jothi, Chemical growth dynamics of 4-Methyl-4′-Hydroxy Benzylidene Aniline NLO single crystal structure and spectroscopic applications, J. Mol. Struct. 1233 (2021) 130054-1-13.
[14] K.H. Lee, S.H. Lee, H. Yun, M. Jazbinsek, J.W. Kim, F. Rotermund, O.P. Kwon, Multi-functional supramolecular building blocks with hydroxy piperidino groups: new opportunities for developing nonlinear optical ionic crystals, Cryst. Eng. Comm. 18 (2016) 5832–5841.
[15] M.R. Anoop, P.S. Binil, S. Suma, M.R. Sudarsanakumar, Y. Sheena Mary, Hema Tresa Varghese, C. Yohannan Panicke, Vibrational spectroscopic studies and computational study of ethyl methyl ketone thiosemicarbazone, J. Mol. Struct. 969 (2010) 48–54.
[16] Sadia Afrin Dalia, Farhana Afsan, Md.Saddam Hossain, Md.Nuruzzaman Khan, C.M. Zakaria, Kudrat-E-Zahan Md., Mohsin Ali Md., A short review on chemistry of schiff base metal complexes and their catalytic application, Int. J. Chem. Stud. 6 (2018) 2859–2866.
[17] A. Olajire Adegoke, Analytical, Biochemical and Synthetic Applications of Para-Dimethylaminobenzaldehyde, Int. J. Pharm. Sci. Rev. Res. 11 (2011) 17–29.
[18] Rasel Das, Eaqub Ali Md, Sharifah Bee Abd Hamid, Current Applications of X-Ray Powder Diffraction- a review, Rev. Adv. Mater. Sci. 38 (2014) 95–109.
[19] Y. Waseda, E. Matsubara, K. Shinoda, X-Ray Diffraction Crystallography: Introduction, Examples and Solved Problems, Springer, 2011.
[20] V. Pecharsky, P. Zavalij, Fundamentals of Powder Diffraction and Structural Characterization of Materials, Second Edition, Springer, 2009.
[21] P.G. Bruce, Powder Diffraction: Theory and Practice, ed., Royal Society of Chemistry, 2008.
[22] J. Reibenspies, A. Clearfield, N. Bhuvanesh, Principles and Applications of Powder Diffraction, Wiley-Blackwell, 2008.
[23] C. Kittel, Introduction to Solid State Physics, John Wiley & Sons, 1996.
[24] B.D. Cullity, Elements of X-Ray Diffraction, Addison-Wesley, Cop., Massachusetts, 1978.
[25] S.K. Kurtz, T.T. Perry, A Powder Technique for the Evaluation of Nonlinear Optical Materials, J. Appl. Phys. 39 (1968) 3798–3813.
[26] W. Hernandez, J. Paz, A. Varisberg, E. Spodinc, R. Richter, Beyer v, Synthesis, Characterization, and In Vitro Cytotoxic Activities of Benzaldehyde Thiosemicarbazone Derivatives and Their Palladium(II) and Platinum(II) Complexes against Various Human Tumor Cell Lines, Bioinorg. Chem. Appl. (2008) 690952-1-10.
[27] I. Dilovic, M. Rubcic, V. Vrdoljak, S.K. Pavelic, M. Kralj, I. Piantanida, M. Cindric, Novel thiosemicarbazone derivatives as potential antitumor agents: Synthesis, physicochemical and structural properties, DNA interactions and antiproliferative activity, Bioorg. Med. Chem. 16 (2008) 5189–5198.
[28] K. Alomar, M.A. Khan, M. Allain, G. Bouet, Synthesis, crystal structure and characterization of 3-thiophene aldehyde thiosemicarbazone and its complexes with cobalt (II), nickel (II) and copper (II), Polyhderon 28 (2009) 1273–1280.
[29] M.C. Rodriguez-Arguelles, P. Touron-Touceda, R. Cao, A.M. Garcia-Deibe, P. Pelgatti, C. Pelizzi, F. Zani, Complexes of 2-acetyl-gamma-butyrolactone and 2-furancarbaldehyde thiosemicarbazones: antibacterial and antifungal activity, J. Inorg. Biochem. 103 (2009) 35–42.
[30] H. Arslan, U. Florke, N. Kulcu, G. Binzet, The molecular structure and vibrational spectra of 2-chloro-N-(diethylcarbamothioyl) benzamide by Hartree–Fock and density functional methods, Spectrochim. Acta A 68 (2007) 1347–1355.
[31] R.N. Jayaprakash, P. Sundaramoorthi, N. Dinesh Babu, Investigations on the Synthesis, Growth and Characterization of Thiosemicarbazone Complex Crystal, *Int. j.* curr. res. *Chem.* 1 (2014) 172–177.
[32] N.P.G. Roeges, A Guide to the Complete Interpretation of Infrared Spectra of Organic Structures, Wiley, New York, 1994.
[33] Colthup N.B., Daly L.H., Wiberly S.E., Introduction to Infrared and Raman Spectroscopy, third edition, 1990.
[34] E.J. Baran, I. Viera, M.H. Torre, Vibrational spectra of the Cu(II) complexes of L-asparagine and L-glutamine, Spectrochim. Acta A 66 (2007) 114–117.
[35] J. Edler, R. Pfister, V. Pouthier, C. Falvo, P. Hamm, Direct Observation of Self–Trapped Vibrational States in α-Helices, Phys. Rev. Lett. 93 (2004) 106405-1-4.
[36] I. Yalcin, E. Sener, O. Ozden, A. Akin, Synthesis and microbiological activity of 5-methyl-2-[*p*-substituted phenyl]benzoxazoles Synthèse et activité microbiologique de 5-méthyl-2-phényl benzoxazoles substitués en para, Eur. J. Med. Chem. 25 (1990) 705–708.
[37] R. Saxena, L.D. Kandpaul, G.N. Mathur, Synthesis and characterization of poly(benzobisthiazole)s derived from halogenated phthalic acid and isophthalic acid, Polym. Sci., Part A: Polym. Chem. 40 (2002) 3959–3966.
[38] A.S. Anwar El-Shahawy, S.M. Ahmed, N.K. Sayed, INDO/SCF-CI calculations and structural spectroscopic studies of some complexes of 4-hydroxyacetanilide, Spectrochim. Acta A 66 (2007) 143–152.
[39] L. Latheef, M.R.P. Kurup, Spectral and structural studies of copper (II) complexes of thiosemicarbazones derived from salicylaldehyde and containing ring incorporated at N (4)-position, Spectrochim. Acta A 70 (2008) 86–93.
[40] G. Socrates, Infrared Characteristic Group Frequencies, John Wiley and Sons, New York, 1980.
[41] K.O. Ferraz, S.M.S.V. Wardell, J.L. Wardell, S.R.W. Louro, H. Beraldo, Copper(II) complexes with 2-pyridineformamide-derived thiosemicarbazones: Spectral studies and toxicity against *Artemia salina*, Spectrochim. Acta A 73 (2009) 140–145.

[42] G. Varsanyi, Assignments For Vibrational Spectra of Seven Hundred Benzene Derivatives, Wiley, New York, 1974.
[43] G.F.S. Andrade, L.J.A. Siqueira, M.C.C. Ribeiro, O. Sala, M.L.A. Temperini, Resonance Raman effect of ferrocene and formylferrocene thiosemicarbazone, J. Raman Spectrosc. 37 (2006) 498–507.
[44] H.A. Badran, M.F. Mudhaffer, Q.M. Hassan, A.Y. Ahmad, Study of the linear optical properties and surface energy loss of 5',5''-dibromo-ocresolsulfophthalein thin films, Chalcogen. Lett. 9 (2012) 483–493.
[45] J. Tauc, Optical properties of amorphous semiconductors, Amorph. Liquid Semicond. (1974) 159–220.
[46] F. Urbach, The long-wavelength edge of photographic sensitivity and of the electronic absorption of solids, Phys. Rev. 92 (1953) 1324.
[47] A. Dhanaraj, K. Das, J.M. Keller, A Study of The Optical Band Gap Energy and Urbach Energy of Fullerene (C60) Doped PMMA Nanocomposites, AIP Conf. Proc. 2270 (2020) 110040-1-5.
[48] K. Elangovan, A. Senthil, G. Vinitha, Growth, structure perfection and characterization of 2-methylimidazolium hydrogen oxalate dihydrate (2MIO) single crystal for NLO applications, J. Mater. Sci. Mater. Electron. 30 (2019) 1–11.
[49] N. Sinha, B.K. Sahas, K. Singh, N. Kumar, M.K. Singh, G.C. Gupta, B. Budakoti, Kumar, Solution growth and comparative characterization of L-HFB single crystals, Cryst. Res. Technol. 44 (2009) 167–172.
[50] M.C. Sreenath, I. Hubert Joe, V.K. Rastogi, Third-order optical nonlinearities of 1,5-Diaminoanthraquinone for optical limiting application, Opt. Laser Technol. 108 (2018) 218–234.
[51] Lakowicz J.R., Principles of Fluorescence Spectroscopy, 3rd edition, 2006.
[52] L. Schermelleh, R. Heintzmann, H. Leonhardt, A guide to super-resolution fluorescence microscopy, J. Cell Biol. 190 (2010) 165–175.
[53] Said Figueredo Lopeza, Manuel Paez Mezaa, Francisco Torres Hoyos, Study of the nonlinear optical properties of 4-nitroaniline type compounds by density functional theory calculations: Towards new NLO materials, Comput. Theor. Chem. 1133 (2018) 25–32.
[54] Landau L.D., Lifshitz E.M., in Electrodynamics of Continuous Media, Second Edition, 8 (1984) 372–393.
[55] R. Sankar, C.M. Raghavan, R. Mohan Kumar, R. Jayave, Growth and characterization of a new semiorganic non-linear optical thiosemicarbazide cadmium chloride monohydrate ($Cd(NH_2NHCSNH_2)C_{l2}$-H_2O) single crystals, J. Cryst. Growth 305 (2007) 156–161.
[56] M. Anis, M.I. Baig, S.S. Hussaini, M.D. Shirsat, Mohd Shkir, H.A. Ghramh, Linear and nonlinear optical analysis on semiorganic *L*-proline cadmium chloride single crystal, Chin. Phys. B 27 (2018) 047801-1-8.
[57] S.P. Ramteke, M.I. Baig, M. Shkir, S. Kalainathan, M.D. Shirsat, G.G. Muley, Mohd Anis, Novel report on SHG efficiency, Z-scan, laser damage threshold, photoluminescence, dielectric and surface microscopic studies of hybrid inorganic ammonium zinc sulphate hydrate, Opt. *Laser* Technol. 104 (2018) 83–89.
[58] Peter J. Haines, Thermal Methods of analysis: principles, Applications and Problems, Springer Science & Business Media, 2012.
[59] Poorja Gill, Tahereh Tohidi Moghadam, Bijan Ranjbar, Differential Scanning Calorimetry Techniques: Applications in Biology and Nanoscience, J. Biomol Tech. 21 (2010) 167–193.
[60] Sara Drissi, Anissa Eddhahak, Sabine Care, Jamel Neji, Thermal analysis by DSC of Phase Change Materials, study of the damage effect, J. Build. Eng. 1 (2015) 13–19.
[61] Peter Borocz, Renata Pidl, Barnabas Toth, Thermo-Analytical Technique to Analize the Quality of Paper for Packaging, J. Appl. Packag. Res. 8 (2016) 31–37.
[62] Jose M. Fernandez, Cesar Plaza, Alfredo Polo, Alain F. Plante, Use of thermal analysis techniques (TG–DSC) for the characterization of diverse organic municipal waste streams to predict biological stability prior to land application, Waste Management 32 (2012) 158–164.
[63] Jihui Ni, Hu Jia, Wanfen Pu, Hang Jiang, Jianjun Yang, Qiang Ren, Thermal kinetics study of light oil oxidation using TG/DTG techniques, J. Therm. Anal. Calorim. 117 (2014) 1349–1355.
[64] S. Mohapatra, N. Mohanty, B.N. Guru, N.C. Pal, The synthesis and FTIR, kinetics and TG/DTG/dta study of biopolymers derived from polyurethanes of glycerol modified linseed oil and cardanol based dyes, J. chem. pharm. 6 (2014) 1493–1502.
[65] P. Hemalatha, V. Veeravazhuthi, A. Chandramohan, Synthesis, growth and characterization of Bis S-benzylisothiouronium tetrachlorido zincate (II) a semiorganic nonlinear optical crystal, J. Cryst. Growth 311 (2009) 4317–4322.
[66] F. Guo, F. Wu, Y. Mu, Y. Hu, X. Zhao, W. Meng, J.P. Giesy, Y. Lin, Characterization of organic matter of plants from lakes by thermal analysis in a N2 atmosphere, Sci. Rep. 6 (2016) 1–7.